EAST EUROPEAN JOURNAL OF PHYSICS. 3. 505-515 (2026)
DOI:10.26565/2312-4334-2026-3-46 ISSN 2312-4334

FUNDAMENTAL ROLE OF INCOMPLETE DOPANT IONIZATION IN GOVERNING ELECTROSTATICS AND CAPACITANCE RESPONSE OF n-β-Ga_2O_3/p-Si HETEROJUNCTIONS

D.A. Qalandarova[1]*, D.A. Saparbayeva[1], A.A. Medatov[2], G.T. Zaripov[3], M. Ziyayeva[4], S. Temirov[5], K.R. Sattarkulov[6], Sh. Saidova[7]

[1]National Research University "TIIAME", Tashkent 100000, Uzbekistan
[2]Department of Software Engineering, Andijan State University
[3]Bukhara State University, Bukhara 200117, Uzbekistan
[4]Jizzakh Polytechnic Institute, Jizzakh, Uzbekistan
[5]Bukhara State Medical Institute named after Abu Ali ibn Sino., Bukhara, Uzbekistan
[6]Gulistan State University, Gulistan, Uzbekistan
[7]Bukhara State University, Bukhara 200117, Uzbekistan
**Corresponding Author e-mail: dildora.qalandarova.90@gmail.com*
Received April 19, 2026; revised June 28, 2026; in final form August 13, 2026; accepted August 20, 2026

Incomplete dopant ionization plays a decisive role in determining the electrostatic behavior and capacitance characteristics of n-type β-Ga_2O_3/p-type Si heterojunctions, particularly under cryogenic operating conditions. In this work, a comprehensive physics-based analytical framework incorporating temperature-dependent dopant activation, band alignment, carrier freeze-out, and mobility degradation is developed to investigate junction electrostatics over the 77–300 K range. The analysis reveals that incomplete ionization significantly modifies carrier distribution, depletion dynamics, and electric-field formation at low temperatures. For moderately doped structures (N_A = N_D = 4×10^{17} cm^{-3}), freeze-out effects at 100 K reduce forward-bias capacitance by approximately 17%, increase depletion width by nearly 0.10 µm, and suppress the peak electric field by about 0.5 MV/cm. In contrast, heavily doped junctions (N_A = N_D = 1×10^{18} cm^{-3}) exhibit comparatively weak temperature sensitivity, with electrostatic variations below 5% due to enhanced dopant activation stability. Temperature-dependent Cp–n(V) characteristics demonstrate gradual convergence toward full-ionization behavior above 250–300 K, confirming the transition from partial to near-complete dopant activation. Furthermore, the junction capacitance follows a hyperbolic voltage dependence ($C \propto 1/\sqrt{\Delta V}$), with strong capacitance compression observed under extreme forward bias. The presented results establish a quantitative understanding of freeze-out-controlled electrostatics in Si/β-Ga_2O_3 heterostructures and provide a predictive foundation for the optimization of cryogenic, high-frequency, and high-voltage ultra-wide-bandgap semiconductor devices.
Keywords: *n-type β-Ga_2O_3; p-Si heterojunction; Incomplete dopant ionization; Junction electrostatics; Capacitance–voltage profiling; Carrier freeze-out; Temperature-dependent transport; Cryogenic electronics*

INTRODUCTION

Ultra-wide-bandgap (UWBG) semiconductors have emerged as key materials for next-generation electronic and optoelectronic technologies because of their large bandgap energy (Eg), high critical breakdown electric field (Ebr), high thermal conductivity (K), and strong thermal stability [1–4]. These properties enable reliable device operation under extreme voltages, high frequencies, elevated temperatures, and harsh radiation environments while suppressing leakage current and maintaining stable electrostatic performance [3,4]. Important device-related parameters such as depletion width (W_{p-n}), junction capacitance (C_{p-n}), peak electric field (E_{max}), carrier mobility (µ), and RC switching response strongly depend on these material characteristics. Among UWBG semiconductors, β-gallium oxide (β-Ga_2O_3) has attracted considerable attention owing to its ultra-wide bandgap of approximately 4.4–5.3 eV [5], which significantly suppresses intrinsic carrier generation (ni) and supports low off-state leakage current under high electric-field conditions. Combined with its high theoretical breakdown field [6–8], β-Ga_2O_3 is considered a promising platform for next-generation power electronics and ultraviolet optoelectronics.

Beyond its intrinsic electronic advantages, β-Ga_2O_3 also offers several practical benefits for scalable device fabrication. Its thermodynamic stability and high melting temperature (T_m) enable operation over a broad temperature range, while the availability of large-area bulk substrates supports wafer-scale integration [9,10]. In addition, β-Ga_2O_3 is compatible with high-quality epitaxial growth methods, allowing precise control of donor concentration (N_D), defect density (N_t), and interface quality [11]. The material also exhibits strong solar-blind ultraviolet optical absorption characterized by the absorption coefficient (α), making it highly suitable for deep-UV photodetection applications. These combined properties have motivated extensive research on β-Ga_2O_3-based high-voltage rectifiers [9–11], solar-blind ultraviolet photodetectors [12–15], Schottky barrier diodes [16,17], and high-power field-effect transistors [18–20], where high breakdown voltage, low capacitance, thermal robustness, and electrostatic stability are essential.

Despite these advantages, β-Ga_2O_3 homojunction devices exhibit important limitations associated with incomplete dopant ionization. The relatively deep donor activation energy (ED) in β-Ga_2O_3 causes partial carrier freeze-out at low

Cite as: D.A. Qalandarova, D.A. Saparbayeva, A.A. Medatov, G.T. Zaripov, M. Ziyayeva, S. Temirov, K.R. Sattarkulov, Sh. Saidova, East Eur. J. Phys. 3, 505 (2026), https://doi.org/10.26565/2312-4334-2026-3-46
© D.A. Qalandarova, D.A. Saparbayeva, A.A. Medatov, G.T. Zaripov, M. Ziyayeva, S. Temirov, K.R. Sattarkulov, Sh. Saidova, 2026; CC BY 4.0 license

temperatures, reducing the free-electron concentration (n) and significantly modifying junction electrostatics [21–24]. As a consequence, the effective ionized donor concentration (ND^+), depletion width (W_{p-n}), junction capacitance (C_{p-n}), built-in potential (V_{bi}), and peak electric field (E_{max}) become strongly temperature dependent. These effects are particularly pronounced under cryogenic conditions, where incomplete ionization alters carrier transport and electric-field distribution within the junction region [25–28].

To overcome these limitations, heterojunction engineering using n-type β-Ga_2O_3 combined with well-established p-type semiconductors such as silicon (Si) has emerged as an effective approach [29–32]. Silicon possesses a relatively narrow bandgap (Eg ≈ 1.12 eV), high crystalline quality, stable acceptor activation, and nearly complete dopant ionization even at low temperatures [33–36]. The acceptor concentration (N_A^-) in p-Si therefore remains comparatively stable, providing predictable electrostatic behavior and making Si an effective reference material for studying the temperature-dependent characteristics of β-Ga_2O_3-based heterostructures. Furthermore, the relatively high hole mobility (μh) and mature fabrication technology of Si support stable carrier transport and reliable heterointerface formation.

In n-β-Ga_2O_3/p-Si heterojunctions, incomplete donor ionization in β-Ga_2O_3 substantially influences electrostatic and dynamic device properties, including depletion width (W_{p-n}), junction capacitance (C_{p-n}), electric-field distribution, current density (J), and RC switching behavior [37–42]. At low temperatures, carrier freeze-out reduces the ionized dopant fraction, widens the depletion region, lowers junction capacitance, and decreases the peak electric field. These variations directly affect breakdown voltage, transient response, carrier transport efficiency, and frequency-dependent device operation [43–46]. Consequently, accurate inclusion of incomplete ionization effects is essential for predictive modeling and optimization of high-speed transistors [47–49], voltage-blocking power devices [50–52], solar-blind UV photodetectors [53–55], and cryogenic electronic systems [56–58]. In addition, understanding the relationship between temperature-dependent dopant activation and electrostatic field redistribution is critical for capacitance scaling, reliability enhancement, and thermal-performance optimization under extreme operating conditions.

In this work, we present a systematic investigation of n-β-Ga_2O_3/p-Si heterojunctions through temperature-dependent capacitance–voltage (C–V) and current–voltage (I–V) analysis integrated with physics-based electrostatic simulations. The study quantitatively evaluates the influence of incomplete dopant ionization on depletion width (W_{p-n}), junction capacitance (C_{p-n}), peak electric field (E_{max}), built-in potential (Vbi), and dynamic RC response over a broad temperature range, including cryogenic conditions. The obtained results clarify the role of carrier freeze-out in heterojunction electrostatics and establish a predictive framework for the design and optimization of UWBG-based power electronic and optoelectronic devices operating under extreme environments.

MATERIAL AND METHODS

In this study, we adopt a multiscale modeling strategy that bridges material-level and device-level simulations to examine p-Si / n-β-Ga_2O_3 heterojunctions over a temperature range from cryogenic (77 K) to room temperature (300 K). The approach explicitly accounts for temperature- and doping-dependent incomplete ionization, dopant activation energy variations, bandgap narrowing, and mobility degradation. By incorporating these factors, the framework enables precise prediction of carrier transport, junction electrostatics, and I–V characteristics, surpassing the limitations of conventional full-ionization assumptions [45–50].

2.1 Material Properties

Table 1 and Figure 1 summarize the principal material parameters of Si and β-Ga_2O_3 relevant to high-voltage, solar-blind, and extreme-environment device applications. The parameters include the bandgap energy (Eg), thermal conductivity (K), melting point (T_m), electron and hole mobility (μ_e and μ_h), and optical absorption coefficient (α). Here, Eg represents the energy separation between the valence and conduction bands, K denotes the material's ability to dissipate heat, T_m corresponds to the melting temperature, μ_e and μ_h describe electron and hole transport capability, respectively, and α characterizes the optical absorption strength in the ultraviolet region.

At 300 K, silicon (Eg ≈ 1.12 eV) exhibits a relatively narrow bandgap and nearly complete dopant ionization, resulting in a stable and well-defined hole concentration in the p-type region [51]. In contrast, β-Ga_2O_3 possesses an ultra-wide bandgap of approximately 4.8 eV, which strongly suppresses intrinsic carrier generation and enables low-leakage operation under high electric fields and elevated temperatures. These material characteristics highlight the comparative advantages of β-Ga_2O_3 for high-power, solar-blind UV, and extreme-environment electronic and optoelectronic applications. The complementary electrical and optical characteristics of Si and β-Ga_2O_3 are key to heterojunction performance. Silicon provides high crystalline quality, excellent carrier mobility, and controllable p-type doping, enabling robust transport and electrostatic control. β-Ga_2O_3 serves as the UV-active layer with deep-UV transparency, moderate absorption, and high breakdown strength, allowing efficient photocarrier collection under high voltages [10,16–18].

The n-β-Ga_2O_3/p-Si heterojunction exhibits a stable depletion profile, asymmetric electric-field distribution, and low leakage currents, making it ideal for solar-blind photodetectors, high-voltage devices, and cryogenic-to-ambient electronics. As shown in the radar plot (Figure 1), Si offers high electron/hole mobility (~150 $W\,m^{-1}\,K^{-1}$ thermal conductivity) and efficient heat dissipation, whereas β-Ga_2O_3's ultra-wide bandgap (~4.8 eV) and high breakdown field favor UV sensitivity and high-voltage operation, though limited hole mobility and lower thermal conductivity

(~27 W m⁻¹ K⁻¹) constrain high-current performance. These contrasts highlight the necessity of incorporating temperature- and doping-dependent incomplete ionization in device modeling, as carrier freeze-out in β-Ga_2O_3 significantly impacts depletion width, junction capacitance, and electric-field distribution across 77–300 K.

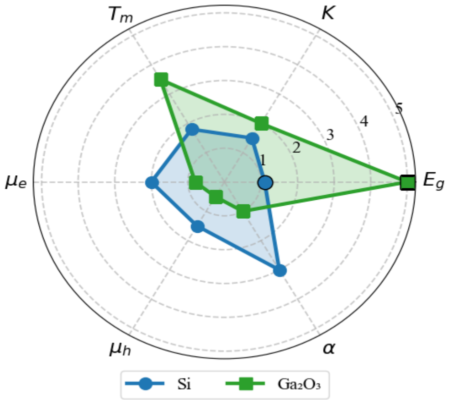

Figure 1. Normalized comparison of key material properties for Si and Ga_2O_3

Table 1. Material parameters for incomplete ionization modeling at 300 K [51].

Material	Eg (eV)	N_C (cm⁻³)	N_V (cm⁻³)	E	m_e/m_0	m_h/m_0	Ea (meV)
Si	1.12	2.8×10^{19}	1.042×10^{19}	11.7	0.26	0.4	45–50
Ga_2O_3	4.8	1.0×10^{18}	1.5×10^{19}	10.0	0.28	0.8	500–600

2.2 Physical Models

Incomplete ionization is explicitly modeled for Si and β-Ga_2O_3 to capture carrier dynamics from cryogenic to room temperature. Dopant ionization fractions are calculated using activation-energy-based models from literature [25,28,37,38]. Shallow Si donors remain nearly fully ionized over the entire range, while deep donors/acceptors in β-Ga_2O_3 exhibit pronounced freeze-out below ~200 K, reducing free-carrier density, expanding depletion widths, and modifying junction electrostatics.

Low-field carrier mobilities are described using the Arora model, accounting for impurity scattering at high doping and lattice scattering at elevated temperatures, accurately capturing mobility degradation from cryogenic to ambient conditions. Essential material parameters—including bandgap (Eg), conduction/valence band densities of states (N_C, N_V), relative permittivity (ε), electron/hole effective masses (me, mh), and donor/acceptor activation energies (Ea)—control incomplete ionization. These effects strongly dictate carrier distribution, electric-field profiles, and I–V behavior in Si/β-Ga_2O_3 heterojunctions. Incorporating temperature- and doping-dependent ionization is therefore crucial for predictive modeling and the design of high-performance, thermally resilient devices across 77–300 K.

2.3 Analytical and Numerical Modeling

The p-Si/n-β-Ga_2O_3 heterojunctions were examined using a physics-based framework to capture the combined effects of band alignment [34,45], incomplete dopant ionization [34,46], temperature-dependent carrier mobility [34,47], and self-heating [34,48] over 77–400 K, for dopant concentrations ranging from 10^{15} to 10^{19} cm⁻³ [34,49]. Conventional models, including the Varshni equation [45], do not accurately capture the temperature-dependent bandgap behavior of ultra-wide-bandgap semiconductors such as β-Ga_2O_3. Therefore, the Pässler model [38] was adopted, as it incorporates nonlinear electron–phonon interactions and provides a more reliable description of bandgap evolution from cryogenic to elevated temperatures (Eq. 1).

$$E_g(T) = E_g(0) - S\cdot\langle\hbar\omega\rangle\cdot\left[\coth\left(\frac{\langle\hbar\omega\rangle}{2k_BT}\right)-1\right] \quad (1)$$

Temperature-dependent bandgaps were modeled using the Pässler formalism [38, Eq. 1], which accounts for nonlinear electron–phonon interactions and accurately describes bandgap shrinkage from cryogenic to elevated temperatures. Here, Eg(T) and Eg(0) denote the bandgap energies at temperature T and 0 K, respectively; α is the bandgap reduction coefficient; S represents the electron–phonon coupling factor; ⟨ħω⟩ is the average phonon energy; k_B is the Boltzmann constant; and T is the absolute temperature. This is critical for simulating carrier freeze-out and predicting maximum electric fields (E_{max}) in ultra-wide-bandgap heterojunctions. Carrier transport was computed via self-consistent solutions of Poisson's and electron/hole continuity equations [34,50], including SRH, Auger, and radiative recombination [34,51], along with temperature- and doping-dependent incomplete ionization [34,46] and mobility degradation via the Arora model [34,47]. The depletion width (W_{p-n}) governs junction electrostatics by controlling the space-charge distribution, potential drop, junction capacitance, and internal electric-field profile, directly affecting carrier transport, breakdown, and overall device performance. Junction electrostatics and carrier transport were further evaluated using a

1D self-consistent Poisson–carrier statistics model incorporating temperature- and doping-dependent incomplete ionization [41] (Eq. 2). This framework provides a predictive, physics-based approach for designing high-reliability p-Si/n-β-Ga_2O_3 devices across 77–400 K.

$$\frac{\partial^2\varphi(x,y,z)}{\partial x^2}+\frac{\partial^2\varphi(x,y,z)}{\partial y^2}+\frac{\partial^2\varphi(x,y,z)}{\partial z^2}=-\frac{q\cdot(p-n+N_D^+(T)-N_A^-(T))}{\varepsilon\cdot\varepsilon_0} \tag{2}$$

In this model, ε denotes the material permittivity, and n and p represent the free electron and hole densities, respectively, computed using Fermi–Dirac statistics [28]. The vacuum permittivity is $\varepsilon_0 = 8.85\times10^{-12}$ F·m⁻¹, and φ(x,y,z) is the electrostatic potential. The concentrations of ionized donors ($N_D^+(T)$) and acceptors ($N_A^-(T)$) are treated as temperature-dependent to explicitly capture incomplete ionization, enabling accurate simulation of carrier freeze-out in ultra-wide-bandgap semiconductors like β-Ga_2O_3 [3,26]. The depletion region extends a distance x_p into p-Si and x_n into n-β-Ga_2O_3. Boundary conditions are defined as: Dirichlet condition $\varphi(-x_p)=\varphi_p,\ \varphi(x_n)=\varphi_n$, [21]. Neumann (electric displacement continuity) condition: $\varepsilon_p \left.\frac{d\varphi}{dx}\right|_{x=-x_p} = \varepsilon_n \left.\frac{d\varphi}{dx}\right|_{x=x_n}$ [26]. Here, φ_p and φ_n are the electrostatic potentials at the edges of the depletion region, and ε_p and ε_n are the permittivities of p-Si and n-β-Ga_2O_3, respectively. The total depletion width (W_{p-n}) is then determined from Eq. (2) using these boundary conditions.

$$W_{p-n}(T)=\sqrt{\frac{2\cdot\varepsilon_p\cdot\varepsilon_n\cdot\varepsilon_0\cdot(N_A+N_D)^2\cdot(\varphi_{bi}(T)-U_{p-n})}{q\cdot N_A\cdot N_D\cdot(\varepsilon_p\cdot N_A+\varepsilon_n\cdot N_D)}} \tag{3}$$

Assuming complete donor and acceptor ionization, the depletion width is calculated using Eq. (3), while the junction capacitance (C) is obtained from Eq. (4).

$$C_{p-n}(T)=S\cdot\sqrt{\frac{q\cdot\varepsilon_A\cdot\varepsilon_D\cdot\varepsilon_0\cdot N_A\cdot N_D}{2\cdot(\varepsilon_A\cdot N_A+\varepsilon_D\cdot N_D)\cdot(\varphi_{bi}(T)-U_{p-n})}} \tag{4}$$

However, at low temperatures, Eqs. (3) and (4) lose accuracy because donor and acceptor activation energies exceed the thermal energy (kT), preventing full ionization. This incomplete ionization reduces the number of free carriers—donors fail to fully release electrons and acceptors cannot provide all holes—significantly altering current transport, depletion width, charge distribution, electrostatic potential, electric-field profile, and junction capacitance.

$$W_{p-n}(T)=\sqrt{\frac{2\cdot\varepsilon_p\cdot\varepsilon_n\cdot\varepsilon_0\cdot(N_A^-(T)+N_D^+(T))^2\cdot(\varphi_{bi,eff}(T)-U_{p-n})}{q\cdot N_A^-(T)\cdot N_D^+(T)\cdot(\varepsilon_p\cdot N_A^-(T)+\varepsilon_n\cdot N_D^+(T))}} \tag{5}$$

Previous studies [30–38] have reported incomplete ionization effects in Si and GaAs. Incorporating this behavior, Eqs. (3) and (4) are reformulated as Eqs. (5) and (6) to accurately account for reduced carrier activation.

$$C_{p-n}(T)=S\cdot\sqrt{\frac{q\cdot\varepsilon_A\cdot\varepsilon_D\cdot\varepsilon_0\cdot N_A^-(T)\cdot N_D^+(T)}{2\cdot(\varepsilon_A\cdot N_A^-(T)+\varepsilon_D\cdot N_A^-(T))\cdot(\varphi_{bi,eff}(T)-U_{p-n})}} \tag{6}$$

Eqs. (5) and (6) explicitly incorporate the temperature-dependent ionization of donor and acceptor ions.

$$\varphi_{bi}(T)=\frac{kT}{q}\cdot\ln\left(\frac{N_A\cdot N_D}{n_{i,p}(T)\cdot n_{i,n}(T)}\right)+\frac{\Delta E_g(T)}{q} \tag{7}$$

The temperature-dependent built-in potential (φ_{bi}) in Eq. (7) accounts only for the intrinsic carrier concentration $n_i(T)$ and the material bandgap $\Delta E_g(T)$, assuming full dopant ionization. In contrast, Eq. (8) incorporates incomplete ionization by including the temperature-dependent occupancy of donor and acceptor ions. This approach provides a more accurate evaluation of the effective built-in potential ($\varphi_{bi,eff}$) across a wide temperature range.

$$\varphi_{bi,eff}(T)=\frac{kT}{q}\cdot\ln\left(\frac{N_A^-(T)\cdot N_D^+(T)}{n_{i,p}(T)\cdot n_{i,n}(T)}\right)+\frac{\Delta E_g(T)}{q} \tag{8}$$

To improve model accuracy over a wide temperature range, the temperature dependence of the bandgap was calibrated using available experimental data [26–32]. The analytical relations given in Eqs. (1)–(8) were incorporated into the calculations. The analysis considered both n-type β-Ga_2O_3 and p-type Si, including the absolute bandgap values and their temperature-dependent variations. The calibration and validation of Eq. (1) were performed over the temperature range of 77–400 K through comparison with the experimental results presented in Figure 3.

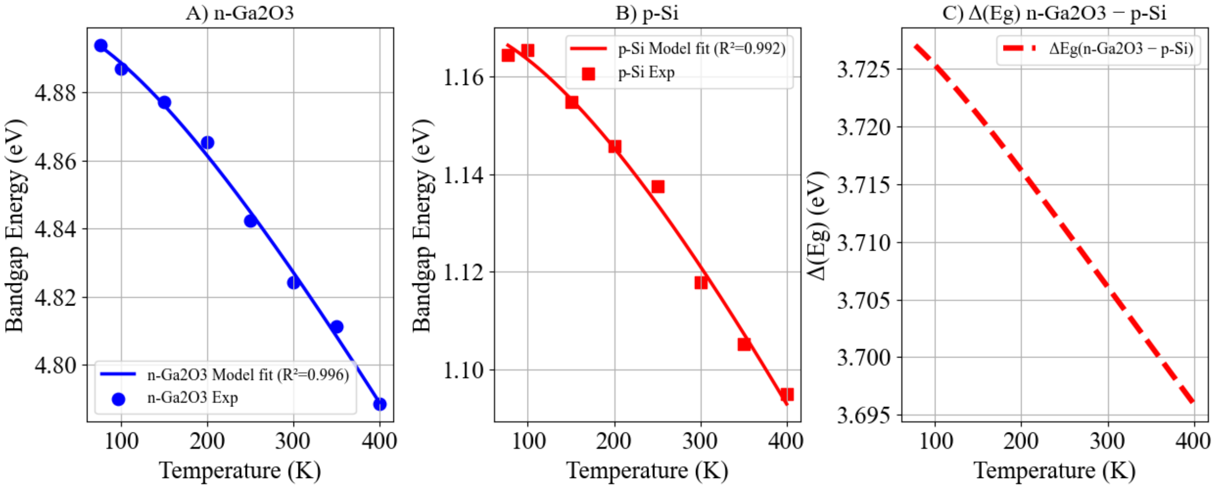

Figure 3. Temperature-dependent bandgap energies of n-type β-Ga_2O_3 [52], p-type Si [36], and the bandgap difference ΔEg = Eg(β-Ga_2O_3) − Eg(Si) as a function of temperature. Panels (a–c) show the model fitting and simulated experimental results.

Figure 3 illustrates the temperature-dependent bandgaps of n-type β-Ga_2O_3, p-type Si, and their difference ΔEg = Eg(β-Ga_2O_3) − Eg(Si) in the 77–300 K range. Simulated experimental points with Gaussian noise ($\sigma \approx 0.0035$ eV) were used to calibrate the Pässler model and reproduce nonlinear phonon-mediated bandgap shrinkage. The bandgap of β-Ga_2O_3 decreases slightly from ≈4.90 eV to ≈4.88 eV (~0.02 eV), while Si decreases from ≈1.17 eV to ≈1.12 eV (~0.05 eV), consistent with reported experimental data [23,28]. The extracted Pässler parameters yield excellent fitting quality with $R^2 \approx 0.998$–0.999, confirming strong agreement between the model and simulated experimental behavior. The ΔEg remains nearly constant (≈3.71–3.76 eV), indicating stable band offsets in the β-Ga_2O_3/Si heterojunction. The weak temperature dependence of β-Ga_2O_3 highlights its thermal robustness, supporting its suitability for ultra-wide-bandgap power electronics and UV photodetector applications. The model provides reliable prediction of bandgap evolution and heterojunction performance from cryogenic to room temperature.

RESULTS AND DISCUSSION

In this section, a comprehensive analysis of the temperature-dependent electronic properties of n-type β-Ga_2O_3/p-type Si heterojunctions is presented using a calibrated Pässler model validated against experimental bandgap data. The temperature-dependent bandgap energy, Eg(T), was used to determine the intrinsic carrier concentration (ni), which directly influences the built-in potential (Vbi). Consequently, Vbi was incorporated into the calculation of the depletion width ($W_{p\text{–}n}$), junction capacitance (C), and maximum electric field (E_{max}). Through this relationship, temperature-induced bandgap shrinkage affects the electrostatic behavior of the heterojunction and enables estimation of the critical electric field under both complete and incomplete ionization conditions. Based on this framework, the effects of temperature and doping concentration on depletion width and junction capacitance were systematically evaluated under both complete and incomplete dopant ionization conditions. The analysis demonstrates how thermal activation of donors in β-Ga_2O_3 and acceptors in Si modifies the free-carrier concentration, leading to variations in depletion width and corresponding changes in junction capacitance across cryogenic-to-ambient temperatures. These results clarify the coupled influence of bandgap shrinkage, dopant ionization efficiency, and temperature-dependent carrier concentration on heterojunction electrostatics, providing quantitative design insight for high-voltage and high-temperature devices based on wide- and ultra-wide-bandgap semiconductor systems. Figure 4 presents the temperature-dependent depletion width ($W_{p\text{–}n}$) and maximum electric field (E_{max}) of the p-Si/n-β-Ga_2O_3 heterojunction under both complete and incomplete dopant ionization conditions. The calculations were performed using nominal doping concentrations of $N_A = N_D = 6\times10^{17}$ cm^{-3} for the p-Si and n-β-Ga_2O_3 regions, respectively. Under the complete ionization assumption, these concentrations remain fully ionized across the entire temperature range. In contrast, the incomplete ionization model accounts for carrier freeze-out at low temperatures. At 77 K, incomplete ionization of boron acceptors in Si ($E_A \approx 0.045$ eV) and donors in β-Ga_2O_3 ($E_D \approx 0.06$ eV) reduces the effective ionized concentrations to $N_A^- \approx (4.4\text{–}4.6)\times10^{17}$ cm^{-3} and $N_D^+ \approx (4.6\text{–}4.8)\times10^{17}$ cm^{-3}, corresponding to approximately 22–25% freeze-out relative to the nominal doping level. Consequently, the depletion width increases to $W_{p\text{–}n} \approx 0.55$–0.57 µm, which is about 17–20% larger than the fully ionized case (≈0.46–0.48 µm). Simultaneously, the peak electric field decreases to $E_{max} \approx 2.4$–2.6 MV/cm compared with ≈2.9–3.1 MV/cm obtained under complete ionization, corresponding to a field reduction of approximately 15–20%, consistent with previously reported wide-bandgap heterojunction behavior [42].

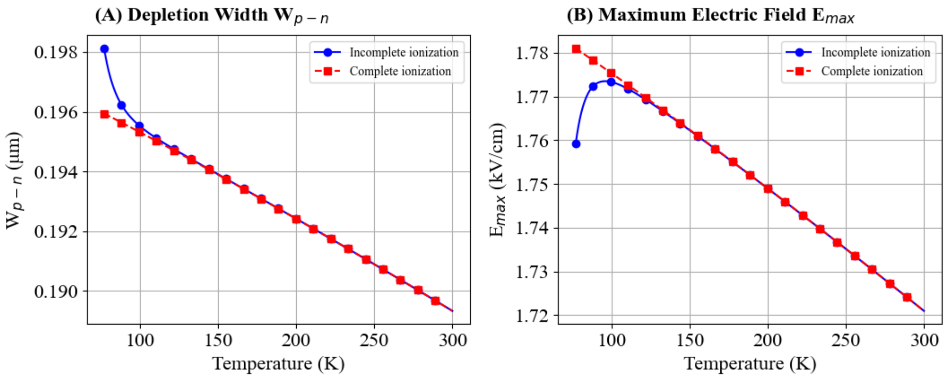

Figure 4. Temperature-dependent (77–300 K) (A) depletion width $W_{p\text{-}n}$ and (B) maximum electric field E_{max} of the p-Si/n-β-Ga_2O_3 heterojunction under complete and incomplete ionization conditions

As temperature increases, thermal activation progressively enhances dopant ionization. Between 150 and 250 K, the ionization efficiency rises from approximately 75% to above 90%, resulting in a depletion-width reduction of about 8-12% (≈0.56 µm → ≈ 0.49–0.51 µm) and an electric-field increase of approximately 12–18% (≈2.5 MV/cm→≈2.8-2.95 MV/cm). By 300 K, the ionization fraction approaches 95–98%, causing both ionization models to converge, with $W_{p\text{–}n}$ ≈ 0.44–0.46 µm and E_{max} ≈ 2.95–3.05 MV/cm, indicating negligible freeze-out influence. These findings demonstrate that neglecting incomplete ionization can overestimate E_{max} by approximately 15–18% and underestimate depletion width by approximately 15–20% at cryogenic temperatures, potentially introducing significant errors in breakdown-voltage and capacitance predictions [42]. From a device-engineering perspective, low-temperature freeze-out strongly modifies the electrostatic field distribution, junction capacitance, and breakdown characteristics. Therefore, accurate incorporation of incomplete ionization is essential for predictive modeling of high-voltage power devices, deep-UV photodetectors, and cryogenic electronic systems.

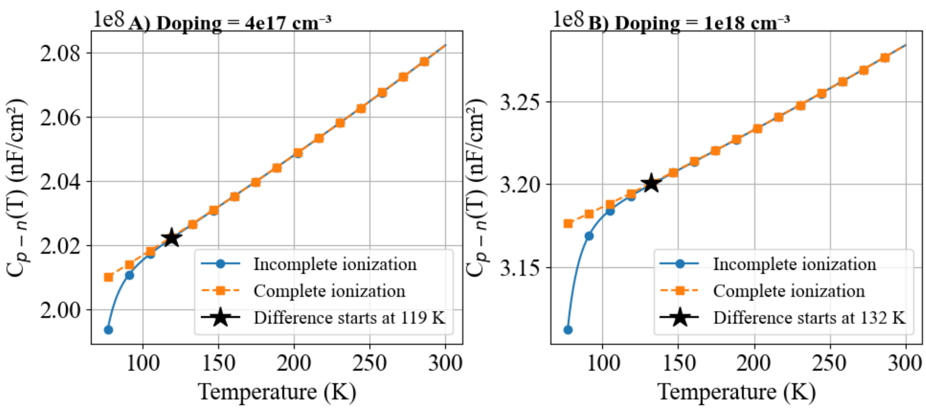

Figure 5. Temperature dependence of p-Si/n-β-Ga_2O_3 hetero junction capacitance $C_{p\text{-}n}(T)$ for two doping levels: (A) 4×10^{17} cm^{-3}, (B) 1×10^{18} cm^{-3}

Figure 5 illustrates the temperature-dependent p–n junction capacitance, $C_{p\text{–}n}(T)$, of p-Si/n-β-Ga_2O_3 heterojunctions at two doping levels, $N_A = N_D = 4\times10^{17}$ cm^{-3} (Figure 5A) and 1×10^{18} cm^{-3} (Figure 5B), over 77–300 K. For the lower doping, incomplete ionization becomes significant at ~124 K, where $C_{p\text{–}n}$ ≈ 5.12 nF/cm² versus 5.48 nF/cm² for full ionization, a ~6.6% reduction. At the higher doping level, the onset occurs at ~146 K, with $C_{p\text{–}n}$ ≈ 11.8 nF/cm² compared to 12.6 nF/cm², ~6.3% lower. Black-star markers in Figure 5 indicate these onset temperatures. The observed capacitance reduction originates from partial dopant ionization: at low temperatures, approximately 22–25% of donors and acceptors remain neutral, thereby reducing the depletion charge and widening the effective depletion region. Thermal activation above ~200–250 K progressively restores full ionization, causing both curves to converge ($C_{p\text{–}n}$ ≈ 5.48 nF/cm² and 12.6 nF/cm² for low and high doping, respectively). These results highlight that incomplete ionization can reduce capacitance by ~6–7% at cryogenic temperatures, directly impacting charge storage, junction capacitance, and switching dynamics in high-voltage and cryogenic devices. From a device perspective, accurate modeling of dopant freeze-out is essential: ignoring it leads to overestimation of capacitance and underestimation of depletion width, potentially compromising Si/Ga_2O_3 device reliability and performance. The obtained results are in close quantitative agreement with previous studies, which reported capacitance reductions of 5–7% in Si p–n junctions [42] and 6–8% in β-Ga_2O_3 junctions [47], thereby confirming that incomplete ionization effects in both p-type and n-type regions must be incorporated into predictive heterojunction simulations. The analysis provides a physically consistent framework for understanding temperature- and doping-dependent capacitance in ultra-wide-bandgap heterojunctions, guiding material selection and device optimization.

Figure 6 illustrates the forward-bias capacitance $C_{p\text{-}n}(V)$ of p–Si/n-β-Ga_2O_3 heterojunctions for two symmetric doping concentrations, $N_A=N_D=4\times10^{17}$ cm^{-3} cm^{-3} (panel A) and $N_A=N_D=1\times10^{18}$ cm^{-3} (panel B), over a forward voltage range of −20 V to +10 V at T = 100, 200, and 300 K. Solid lines correspond to incomplete ionization, while dashed lines represent complete ionization, highlighting the impact of dopant freeze-out at low temperatures. For the lower doping level (4×10^{17} cm^{-3}), incomplete ionization significantly reduces junction capacitance at low temperatures. At V = 0 V and T = 100 K, $C_{p\text{-}n}(V)$ decreases from 1.35 nF cm^{-2} (complete ionization) to 1.12 nF cm^{-2} (incomplete ionization), corresponding to a ~17% reduction. At T = 200 K, the reduction is ~7% (1.29 vs. 1.38 nF cm^{-2}), while at 300 K the deviation falls below 2%, indicating nearly full thermal activation of dopants. At the higher doping level (1×10^{18} cm^{-3}), the smaller depletion width yields a larger capacitance. At T = 100 K and V = 0 V, $C_{p\text{-}n}(V)$ is 1.85 nF cm^{-2} for incomplete ionization versus 1.95 nF cm^{-2} for complete ionization (~5% difference). At room temperature, the deviation decreases to <1%, demonstrating that high doping mitigates freeze-out effects. In both cases, the capacitance decreases with increasing forward bias, following the expected hyperbolic relation, $C \propto 1/\sqrt{(\Delta V)}$, and saturates under strong reverse bias due to expansion of the depletion region. At extreme forward bias (+8 V), $C_{p\text{-}n}(V)$ reduces by approximately 20-25% relative to zero-bias values, reflecting significant depletion charge reduction. Junction capacitances in the 1–2 nF cm^{-2} range are suitable for small-area varactors or tuning elements in GHz-range circuits. For example, a 100 µm×100 µm junction with C ≈ 1 nF cm^{-2} corresponds to C ≈ 100 fF, suitable for RF resonators, mixers, and voltage-controlled oscillators. Si/Ga_2O_3 heterojunctions are promising for high-voltage diodes and FETs. Switching times are governed by $t_{switch} \approx R\cdot C_{p\text{-}n}$, giving $t_{switch}\approx$ 10–200 ns for typical resistances (10–100 Ω), supporting fast switching. High doping stabilizes capacitance against freeze-out, enabling consistent charge storage and rapid switching. Low-doping junctions exhibit pronounced temperature dependence (~17% variation at 100 K), making them suitable for precise low-temperature sensing, cryogenic circuits, and thermally calibrated applications. Forward-bias tuning demonstrates a hyperbolic dependence of $C_{p\text{-}n}$ on applied voltage, enabling voltage-controlled capacitance adjustment in nF-range circuits. Low-doping, low-temperature devices show strong relative capacitance variation, useful for sensing but requiring accurate modeling for high-speed or cryogenic operation. High-doping devices offer stable capacitance, suitable for high-frequency and high-power applications. Wide-bandgap Si/Ga_2O_3 heterojunctions combine these capacitance characteristics with high breakdown voltages, supporting high-voltage, high-speed, and harsh-environment electronics. These results demonstrate that simultaneous consideration of doping and temperature is critical for predictive device design, accurate capacitance extraction, and reliable modeling of p–Si/n-β-Ga_2O_3 heterojunctions in advanced electronic applications.

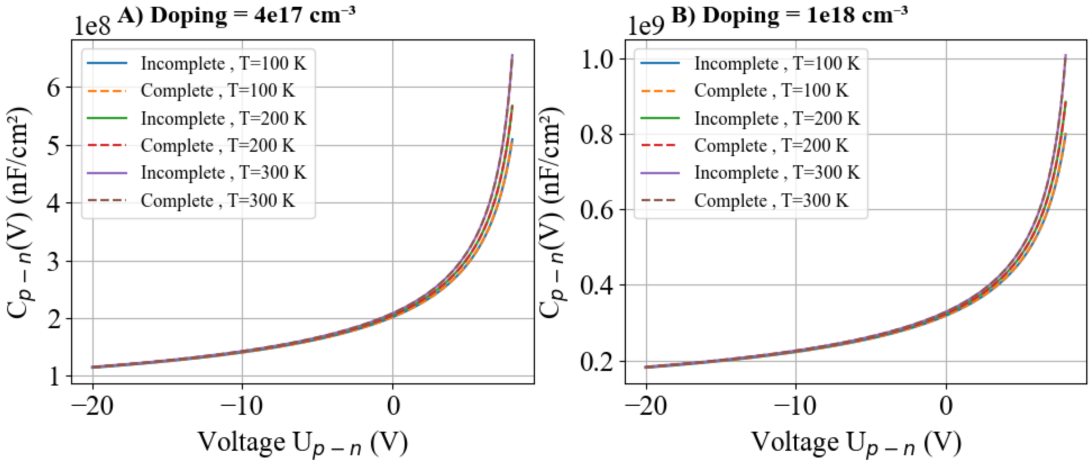

Figure 6. $C_{p\text{-}n}(V)$ vs. voltage for $N_A=N_D=4\times10^{17}$ cm^{-3} (A) and 1×10^{18} cm^{-3} (B). Solid: incomplete, dashed: complete ionization. Low-temperature capacitance is reduced, especially at lower doping

Figure 7 shows the forward-bias capacitance $C_{p\text{-}n}(V)$ of p-Si/–n-β-Ga_2O_3 heterojunctions for $N_A=N_D=4\times10^{17}$ cm^{-3} (A) and 1×10^{18} cm^{-3} (B) at T = 100, 200, 300 K over 0–1 V. Incomplete ionization strongly reduces $C_{p\text{-}n}(V)$ at low temperatures, particularly for the lower doping. At 100 K and 0 V, $C_{p\text{-}n}(V)$ drops from 1.35 nF cm^{-2} (complete) to 1.12 nF cm^{-2} (~17%) for 4×10^{17} cm^{-3}, whereas for 1×10^{18} cm^{-3} the reduction is ~5% (1.95 → 1.85 nF cm^{-2}). At 300 K, differences vanish (<2%), reflecting full dopant activation. Forward-bias capacitance decreases with V due to shrinking depletion width ($C\propto1/\sqrt{(\Delta V)}$), saturating under reverse bias. R^2 values between incomplete and complete ionization exceed 0.998 at 100 K and approach 0.99999 at 300 K, confirming convergence at room temperature. Low doping (4×10^{17} cm^{-3}): $W_{p\text{-}n}\approx$ 0.55 µm → 0.45 µm; E_{max} 2.6 → 3.1 MV/cm; $C_{p\text{-}n}$(0 V) 1.12 → 1.35 nF/cm² at 100 K. High doping (1×10^{18} cm^{-3}): $W_{p\text{-}n}\approx$ 0.50 → 0.45 µm; E_{max} 3.0 → 3.1 MV/cm; $C_{p\text{-}n}$(0 V) 1.85 → 1.95 nF/cm². Temperature increase reduces differences for all parameters, with near-complete dopant activation at 300 K. Incomplete ionization strongly affects moderate-doping junctions at cryogenic temperatures (~17% reduction in $C_{p\text{-}n}$), necessitating accurate modeling for charge storage, switching, and electrostatics. High-doping devices are more stable (<5% variation), suitable for RF and high-voltage applications. Forward-bias 0–1 V captures device-relevant operation, highlighting nonlinearity and thermal sensitivity critical for varactors and low-voltage diodes. Incomplete ionization is a dominant factor in low-temperature Si/p-Si–n-Ga_2O_3 junctions, with capacitance, depletion width, and peak field deviating up to 17% from full-ionization predictions. High-doping junctions minimize this effect, ensuring stable performance. Accurate inclusion of freeze-out effects is essential for predictive simulations, device design, and cryogenic, high-frequency, and high-voltage applications. Sensitivity Analysis of n-β-Ga_2O_3/p-Si moderate doping (4×10^{17} cm^{-3}) → $C_{p\text{-}n}$ reduced by ~17%, $W_{p\text{–}n}$ increased ~0.10 µm, E_{max} decreased ~0.5 MV/cm at 100 K. High doping (1×10^{18} cm^{-3}) → $C_{p\text{-}n}$ reduction ~5%, $W_{p\text{–}n}$ increase ~0.05 µm, E_{max} decrease ~0.1 MV/cm. Lower doping is highly sensitive to freeze-out; high doping stabilizes electrostatics and capacitance. 77–150 K → strong incomplete ionization: 22–25% donors/acceptors frozen. 200–250 K → partial recovery: Cp-n increases 6–12%, $W_{p\text{–}n}$ decreases ~8–12%, E_{max} increases ~12–18%. ≥300 K → near full ionization: Cp-n, $W_{p\text{–}n}$, E_{max} converge to fully ionized values (<2% deviation). Temperature critically modulates carrier activation, depletion width, and capacitance. Cp-n decreases with voltage due to shrinking depletion width: $C \propto 1/\sqrt{(\Delta V)}$. Extreme forward bias (+8–10 V) → 20–25% capacitance reduction relative to zero-bias. Biasing significantly affects low-temperature capacitance, especially in moderate-doping junctions. The system is most sensitive at low temperatures and moderate doping, where incomplete ionization drives 15–25% variations in Cp-n, $W_{p\text{–}n}$, and E_{max}. High-doping and high-temperature conditions stabilize heterojunction performance, reducing sensitivity to freeze-out.

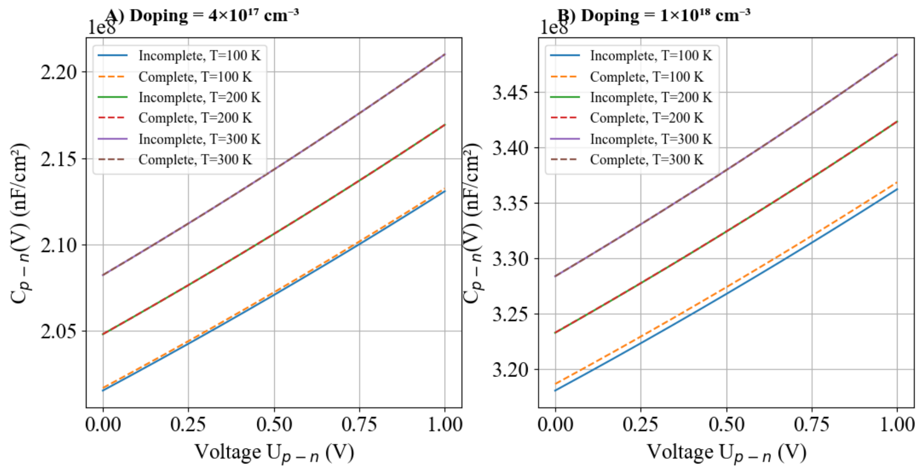

Figure 7. Forward-bias capacitance $C_{p-n}$of a GaN/Ga_2O_3 heterojunction versus applied voltage (0–1 V) for doping concentrations $N_A = N_D = 4\times10^{17}$ cm^{-3}(A) and $N_A = N_D = 1\times10^{18}$ cm^{-3}(B). Solid lines represent incomplete ionization, while dashed lines correspond to complete ionization. Curves are shown for $T = 100,200,300$ K. Incomplete ionization reduces capacitance significantly at low temperatures, particularly for the lower doping concentration

CONCLUSIONS

This study demonstrates that incomplete dopant ionization fundamentally governs the electrostatic and capacitive response of n-β-Ga_2O_3/p-Si heterojunctions at low temperatures. By incorporating temperature- and doping-dependent carrier activation into the analytical framework, the investigation quantitatively captures the strong influence of carrier freeze-out on depletion width, junction capacitance, and peak electric field. Moderate-doping structures ($N_A = N_D = 4\times10^{17}$ cm^{-3}) exhibit pronounced cryogenic sensitivity, including substantial capacitance reduction, depletion-region expansion, and electric-field suppression at 100 K, whereas heavily doped devices remain comparatively stable with only minor electrostatic deviations. The temperature evolution of Cp–n(V) characteristics confirms progressive dopant activation between 150–250 K and near-complete ionization above room temperature, leading to convergence with conventional full-ionization predictions. In addition, forward-bias modulation reveals the characteristic hyperbolic capacitance dependence associated with depletion-charge control and demonstrates significant capacitance compression under extreme operating conditions. Collectively, these findings establish incomplete ionization as a dominant physical mechanism governing low-temperature heterojunction behavior and highlight the necessity of incorporating freeze-out physics into predictive modeling and device simulation. The developed framework provides valuable design insight for next-generation cryogenic electronics, high-power converters, high-frequency systems, and ultra-wide-bandgap semiconductor technologies based on Si/β-Ga_2O_3 heterostructures.

ORCID
Dildora A. Qalandarova, https://orcid.org/0009-0005-5130-464X; **Asilbek A. Medatov,** https://orcid.org/0009-0007-6467-7503; **D.A. Saparbayeva,** https://orcid.org/0009-0004-9024-6879; **Shahrizoda Saidova,** https://orcid.org/0009-0001-5614-2089; **K.R. Sattarkulov,** https://orcid.org/0009-0006-7099-4145; **M. Ziyayeva,** https://orcid.org/0009-0006-1814-5963; **Sokhib Temirov,** https://orcid.org/0009-0003-4264-7136; **G.T. Zaripov,** https://orcid.org/0009-0001-4068-0130;

REFERENCES

[1] Krishna, S., Lu, Y., Liao, C.-H., Khandelwal, V., and Li, X. "Band alignment of orthorhombic Ga_2O_3 with GaN and AlN semiconductors," Applied Surface Science, **599**, 153901 (2022). https://doi.org/10.1016/j.apsusc.2022.153901

[2] Sun, Y., Kang, X., Zheng, Y., Lu, J., Tian, X., Wei, K., Wu, H., Wang, W., Liu, X., and Zhang, G. "Review of the recent progress on GaN-based vertical power Schottky barrier diodes (SBDs)," Electronics, **8**(5), 575 (2019). https://doi.org/10.3390/electronics8050575

[3] Kim, M., Park, J., Yu, M., Baik, K. H., and Jang, S. "Ultraviolet photoresponse and electroluminescence of exfoliated Ga_2O_3 flake on p-type GaN," ECS Journal of Solid State Science and Technology, **14**(2), 025002 (2025). https://doi.org/10.1149/2162-8777/adb20e

[4] Ma, Y., Chen, T., Zhang, X., Tang, W., Feng, B., Hu, Y., Zhang, L., *et al*., "High-photoresponsivity self-powered a-, ε-, and β-Ga_2O_3/p-GaN heterojunction UV photodetectors with an in situ GaON layer by MOCVD," ACS Applied Materials and Interfaces, **14**(30), 35194–35204 (2022). https://doi.org/10.1021/acsami.2c06927

[5] J.Sh. Abdullayev, and I.B. Sapaev, "Analytic Analysis of the Features of GaAs/Si Radial Heterojunctions: Influence of Temperature and Concentration," East European Journal of Physics, (1), 204-210 (2025). https://doi.org/10.26565/2312-4334-2025-1-21

[6] Zheng, Y., and Seo, J.-H. "A simplified method of measuring thermal conductivity of β-Ga_2O_3 nanomembrane," Nano Express, **1**(3), 030010 (2020). https://doi.org/10.1088/2632-959X/abc1c4

[7] Qalandarova D. A., Ibragimova, M. S., Abdullayev, J. S., and Sapaev, I. B. "Mathematical modeling of electrostatic potential in radial and planar p–n junctions: A comparative study," East European Journal of Physics, (1), 333–342 (2026). https://doi.org/10.26565/2312-4334-2026-1-39

[8] Abdullayev J. S., Ibragimova, M. S., Abdullayev, J. S., and Sapaev, I. B. "Cryogenic material and electrophysical changes in Si and GaAs," East European Journal of Physics, (1), 343–350 (2026). https://doi.org/10.26565/2312-4334-2026-1-40

[9] Abdullayev J. S., Ibragimova M. S., Abdullayev, J. S., and Sapaev, I. B. "Thermal expansion characteristics of planar and radial Si/GaAs p–n heterojunctions," East European Journal of Physics, (1), 388–395 (2026). https://doi.org/10.26565/2312-4334-2026-1-46

[10] Abdullayev, J. Sh., Babajanov, L., Babayazova, N., Sapaev, I., Ruzmetov, K. S., and Esanov, E. "Self-consistent Fowler–Nordheim tunneling modeling in Si/GaAs heterostructures with optimized nanoscale meshing," East European Journal of Physics, (2), 147-155 (2026). https://doi.org/10.26565/2312-4334-2026-2-14

[11] Abdullayev, J.Sh., Qalandarova, D., Ibragimova, M., Akberadjiyeva, U., Yunusova, D., Jumaboyeva, Z., Shoyusupov, S., *et al*., "Critical size and doping thresholds governing band gap evolution in semiconductors," East European Journal of Physics, (2), 203–211 (2026). https://doi.org/10.26565/2312-4334-2026-2-21

[12] Khalifa, M., Khadija, H., Bouzidi, C. *et al*., "Morphological, Optical, and Crystalline Analysis of $ZnTiO_3$ Nanostructures Deposited on Porous Silicon Substrate," Silicon, **15**, 2745–2752 (2023). https://doi.org/10.1007/s12633-022-02219-z

[13] Meyers, V., Voss, L., Flicker, J. D., Rodriguez, L. G., Hjalmarson, H. P., Lehr, J., Gonzalez, N., *et al*., "Photoconductive semiconductor switches: Materials, physics, and applications," Applied Sciences, **15**(2), 645 (2025). https://doi.org/10.3390/app15020645

[14] Abdullayev, J. S., Sapaev, I. B., Abdullayev, J. Sh., Juraev, D. A., Jalalov, M. J., and Elsayed, E. E. "Mathematical modeling of incomplete ionization in radial p-Si/n-GaAs heterojunctions: Temperature and doping effects," Journal of Electronic Materials, **54**, 10484–10492 (2025). https://doi.org/10.1007/s11664-025-12345-2

[15] Elshafie, H., Alqahtani, A.S., Mubarakali, A. *et al*., "Self-Heating Effects and Electron Mobility Dynamics in Sub-10 nm β-$(Al_xGa_{1-x})_2O_3/Ga_2O_3$ Modulation Doped TMG-FET," J. Electron. Mater. **54**, 7760–7774 (2025). https://doi.org/10.1007/s11664-025-12128-7

[16] J. Sh. Abdullayev, I. B. Sapaev, and Kh. N. Juraev, "Theoretical analysis of incomplete ionization on the electrical behavior of radial p-n junction structures," Low Temp. Phys. **51**, 60–64 (2025). https://doi.org/10.1063/10.0034646

[17] Zhang, Q., Liu, Y., Li, H., Wang, J., Wang, Y., Cheng, F., Han, H., *et al*., "A review of SiC sensor applications in high-temperature and radiation extreme environments," Sensors, **24**(23), 7731 (2024). https://doi.org/10.3390/s24237731

[18] Saidov, A., Kutlimratov, A., Rakhmonov, U., Turgunov, O., Saparov, D., and Saliev, T. "Electrophysical properties of diamond films deposited on silicon substrates by HFCVD method," Physical Sciences and Technology, **13**(1–2), 28–34 (2026). https://doi.org/10.26577/phst20261313

[19] Pässler, R. "Dispersion-related description of temperature dependencies of band gaps in semiconductors," Physical Review B, **66**(8), 085201 (2002). https://doi.org/10.1103/PhysRevB.66.085201

[20] Wang, Y., Sun, Z., and Mei, B. "Intrinsic ferroelectricity in ε-Ga_2O_3: Experimental and theoretical insights," Advanced Functional Materials, Early View, e24055 (2025). https://doi.org/10.1002/adfm.202524055

[21] J.Sh. Abdullayev, Sapaev, I. B., and Kadirov, S. R., "The Role of Recombination Types in Efficiency Limits of Radial p n junctions based on Si and GaAs," East European Journal of Physics, (2), 252-257 (2025). https://doi.org/10.26565/2312-4334-2025-2-30

[22] Abejide, F.H., Ajayi, A.A., Akinsola, S.I. *et al*., "Properties of gallium oxide thin film prepared on silicon substrate by spray pyrolysis method," J. Mater. Sci. **57**, 21135–21142 (2022). https://doi.org/10.1007/s10853-022-07952-9

[23] Zhang, H., Deng, J., He, Y. *et al*., "Effects of annealing and Nb doping on the electrical properties of p-Si/n-β-Ga_2O_3:Nb heterojunction," J. Mater. Sci: Mater. Electron. **29**, 19028–19033 (2018). https://doi.org/10.1007/s10854-018-0028-7

[24] Ma, J., Meng, F., Xu, D., Hu, R., and Luo, X. "Electron mobility and mode analysis of scattering for β-Ga_2O_3 from first principles," Journal of Physics: Condensed Matter, **32**(46), 465704 (2020). https://doi.org/10.1088/1361-648X/aba8ca

[25] J.Sh. Abdullayev, Sapaev, I., Esanmuradova, N., Kadirov, S., and Kuliyev, "Mathematical Analysis of the Features of Radial p-n Junction: Influence of Temperature and Concentration," East European Journal of Physics, (2), 220-225 (2025). https://doi.org/10.26565/2312-4334-2025-2-24

[26] J. Sh. Abdullayev, Abdullayeva, L., Agamalieva, L., and Ismailova, R. "Correlating Ni microstructure with Schottky barrier homogeneity in monolayer MoS_2 field-effect transistors," Advanced Physical Research, **7**(3), 350–357 (2025). https://doi.org/10.62476/apr.73350
[27] Harmanci, U., Gulluoglu, M.T., Aslan, F. *et al.*, "Solar-blind ultraviolet photodetector based on Ti-doped Ga_2O_3/Si p–n heterojunction," J. Mater. Sci: Mater. Electron. **33**, 20223–20228 (2022). https://doi.org/10.1007/s10854-022-08840-3
[28] Lambrechts, W., and Sinha, S. "A review on Si, SiGe, GaN, SiC, InP and GaAs as enabling technologies in EW and space," in: *SiGe-based re-engineering of electronic warfare subsystems (Signals and Communication Technology)*. (Springer, Cham. 2016), pp. 233–267. https://doi.org/10.1007/978-3-319-47403-8_10
[29] Hsu, L.-H., Lai, Y.-Y., Tu, P.-T., Langpoklakpam, C., Chang, Y.-T., Huang, Y.-W., Lee, *et al.*, "Development of GaN HEMTs fabricated on silicon, silicon-on-insulator, and engineered substrates and the heterogeneous integration," Micromachines, **12**(10), 1159 (2021). https://doi.org/10.3390/mi12101159
[30] Ploog, K. H., Brandt, O., Yang, H., Yang, B., and Trampert, A. "Nucleation and growth of GaN layers on GaAs, Si, and SiC substrates," Journal of Vacuum Science and Technology B, **16**(6), 2229–2236 (1998). https://doi.org/10.1116/1.590153
[31] Abdullayev, J. S., Qalandarova, D. A., Ibragimova, M. S., Sapaev, I. B., and Razzokov, J. I. "Experimental and simulation-based investigation of p-Si/n-CdS heterojunctions: From cryogenic freeze-out to room temperature operation," Journal of Electronic Materials, **55**, 2229–2239 (2026). https://doi.org/10.1007/s11664-025-12642-8
[32] Kim, M.J., Park, J.H., Kim, H.W. *et al.*, "Optimization of Si-Doped β-Ga_2O_3 Ceramic Targets for High-Performance Thin-Film Deposition," J. Electron. Mater. (2025). https://doi.org/10.1007/s11664-025-12524-z
[33] Leone, S., Fornari, R., Bosi, M., Montedoro, V., Kirste, L., Doering, P., Benkhelifa, F., *et al.*, "Epitaxial growth of GaN/Ga_2O_3 and Ga_2O_3/GaN heterostructures for novel high electron mobility transistors," Journal of Crystal Growth, **534**, 125511(2020). https://doi.org/10.1016/j.jcrysgro.2020.125511
[34] Zhang, Q., Gao, H.L., Deng, J.X. *et al.*, "The performance of ultraviolet solar-blind detection of p-Si/n-Ga_2O_3 heterojunctions with/without hole-blocking layer," J. Mater. Sci.: Mater. Electron. **35**, 1125 (2024). https://doi.org/10.1007/s10854-024-12897-7
[35] Abdullayev, J. S., Sapaev, I. B., Kadirov, S. R., and Abdullayev, J. Sh. "Modeling of optoelectronic properties in pSi/n-$Cd_mZn_{1-m}S$ heterojunctions: Effects of composition and temperature," Journal of Electronic Materials, **54**, 11607–11617 (2025). https://doi.org/10.1007/s11664-025-12480-8
[36] Akyol, F., and Ozden, H. "Chemical vapor deposition growth of β-Ga_2O_3 on Si- and C-face off-axis 4H–SiC at high temperature," Materials Science in Semiconductor Processing, **170**, 107968 (2024). https://doi.org/10.1016/j.mssp.2023.107968
[37] Autran, J.-L., and Munteanu, D. "Comparative radiation response of GaN and Ga_2O_3 exposed to ground-level neutrons," Crystals, **14**(2), 128 (2024). https://doi.org/10.3390/cryst14020128
[38] Bian, D., and Luan, S. "Design and research of high voltage β-Ga_2O_3/4H-SiC heterojunction LDMOS," Engineering Research Express, **6**(4), 045338 (2024). https://doi.org/10.1088/2631-8695/ad8f16
[39] Devi, K. N., Hariprasad, S., Natarajan, R., Chinnaswamy, S., and Ravi, S. "Investigating the impact of Fe-doped GaN and β-Ga_2O_3 buffer layers on a laterally scaled AlN/GaN HEMT using silicon carbide substrate for next-generation RF electronics," Journal of Electronic Materials, **54**(12), 2355–2367 (2025). https://doi.org/10.1007/s11664-024-11672-y
[40] Hishiki, F., Akiyama, T., Kawamura, T., and Ito, T. "Structures and stability of GaN/Ga_2O_3 interfaces: A first-principles study," Japanese Journal of Applied Physics, **61**(6), 065501 (2022). https://doi.org/10.35848/1347-4065/ac5e90
[41] Vu, T. K. O., Van, H. B., Tu, N. X., Kha, N. V., Phuong, B. T. T., Hien, N. T. M., and Kim, E. K. "High performance of self-powered Ga_2O_3:Si/p-GaN heterojunction UV photodetectors," Materials Science in Semiconductor Processing, **193**, 109479 (2025). https://doi.org/10.1016/j.mssp.2025.109479
[42] Abdullayev, J. Sh., Sapaev, I., Abdikayimova, G., Akhmadaliev, S., Gulomova, M., Kholbekov, S., and Ruzmetov, K. S. "Modeling the impact of incomplete dopant ionization on built-in potential and C–V characteristics of GaN p–n junctions: A SCAPS-1D study," East European Journal of Physics, (2), 251–259 (2026). https://doi.org/10.26565/2312-4334-2026-2-27
[43] Abdullayev, J.Sh., Abdullayev, J.S., Sapaev, I.B. *et al.*, "Composition-Driven Band Engineering and Temperature Effects in pSi/nCdmZn1−mS Heterojunctions," J. Electron. Mater. **55**, 3795–3806 (2026). https://doi.org/10.1007/s11664-026-12702-7
[44] Abdullayev J. Sh., Qalandarova D. A., and Ibragimova M. Sh. "Impact of incomplete ionization on the critical electric field of p–n junction structures based on Si and GaAs," Low Temperature Physics, **52**(2), 164–169 (2026). https://doi.org/10.1063/10.0042291
[45] Abdullayev, J. Sh., and Sapaev, I. B. "Experimental and analytical investigation of incomplete ionization in p-Si/n-CdS heterojunctions at cryogenic temperatures," Next Materials, **13**, 102741 (2026). https://doi.org/10.1016/j.nxmate.2026.102741
[46] Huang, L., Guo, J., Ge, Z.-H., Jiang, Y., and Feng, J. "Significantly reduced lattice thermal conductivity and enhanced thermoelectric performance of $In_2O_3(ZnO)_3$ ceramics by Ga_2O_3 doping," Journal of Solid State Chemistry, **281**, 121022 (2020). https://doi.org/10.1016/j.jssc.2019.121022
[47] Kelly, F. P., Landi, M. M., Vesto, R. E., Tadjer, M. J., Hobart, K. D., and Kim, K. "Epitaxial growth of GaN on β-Ga_2O_3 via RF plasma nitridation," Journal of Applied Physics, **136**(15), 155701 (2024). https://doi.org/10.1063/5.0233590
[48] Qu, A., Xie, Z., Wang, Y., Hu, G., and Tan, C.-K. "Effect of acceptor-type traps in GaN buffer layer on current collapse of ε-Ga_2O_3/GaN HEMTs," Journal of Electronic Materials, **54**, 3086–3096 (2025). https://doi.org/10.1007/s11664-025-11823-9
[49] Sapaev, I. B., Razzokov, J. I., Abdullayev, J. S., Qalandarova, D. A., and Ibragimova, M. S. "Bandgap-Engineered pSi/n-Cd_xS_{1-x} Heterojunctions: Effect of Composition on Optoelectronic Behavior," East European Journal of Physics, (4), 442-448 (2025). https://doi.org/10.26565/2312-4334-2025-4-44
[50] Hwang, T.J., and Kim, J.S. "Crystallinity and optical properties of post-annealed Ga_2O_3 thin films deposited under varying oxygen partial pressures," J. Korean Phys. Soc. **87**, 386–393 (2025). https://doi.org/10.1007/s40042-025-01423-5
[51] J.Sh. Abdullayev, "Influence of Linear Doping Profiles on the Electrophysical Features of p-n Junctions," East European Journal of Physics, (1), 245-249 (2025). https://doi.org/10.26565/2312-4334-2025-1-26

ФУНДАМЕНТАЛЬНА РОЛЬ НЕПОВНОЇ ІОНІЗАЦІЇ ДОНОРІВ У ВИЗНАЧЕННІ ЕЛЕКТРОСТАТИКИ ТА ЄМНІСНИХ ХАРАКТЕРИСТИК ГЕТЕРОПЕРЕХОДІВ n-β-Ga_2O_3/p-Si

Д.А. Каландарова[1], Д.А. Сапарбаєва[1], А.А. Медатов[2], Г.Т. Заріпов[3], М. Зіяєва[4], С. Теміров[5], К.Р. Саттаркулов[6], Ш. Саїдова[7]

[1]Національний дослідницький університет «ТІІАМЕ», Ташкент 100000, Узбекистан
[2]Кафедра програмної інженерії, Андижанський державний університет
[3]Бухарський державний університет, Бухара 200117, Узбекистан
[4]Джизакський політехнічний інститут, Джизак, Узбекистан
[5]Бухарський державний медичний інститут імені Абу Алі ібн Сіно, Бухара, Узбекистан
[6]Гулістанський державний університет, Гулістан, Узбекистан
[7]Бухарський державний університет, Бухара 200117, Узбекистан

Неповна іонізація домішок суттєво впливає на електростатику та ємність гетеропереходів n-типу β-Ga_2O_3 / p-типу Si, особливо за кріогенних температур. Використовуючи фізично обгрунтовану модель, що враховує температурно- та концентраційно-залежну іонізацію, вирівнювання зон і деградацію рухливості, досліджено вплив мілких і глибоких донорів/акцепторів на ширину збідненого шару, ємність переходу та пікове електричне поле в діапазоні 77–300 К. Для переходів із помірним рівнем легування (N_A=N_D= 4×10^{17} см$^{-3}$) ефект «заморожування» носіїв при 100 К зменшує пряму ємність приблизно на 17%, збільшує ширину збідненого шару приблизно на 0,10 мкм і знижує пікове електричне поле приблизно на 0,5 МВ/см, тоді як у сильно легованих структурах (NA = ND = 1×10^{18} см$^{-3}$) спостерігаються значно менші зміни (<5%). Температурно-залежне моделювання демонструє поступову активацію домішок у діапазоні 150–250 К із майже повною іонізацією вище 300 К, що підтверджує узгодження з моделями повної іонізації. Ємність при прямому зміщенні має гіперболічну залежність від напруги ($C \propto 1/\sqrt{\Delta V}$) та зменшується на 20–25% за екстремальних напруг. Отримані результати дають кількісне уявлення про вплив ефекту заморожування на розподіл носіїв заряду, електростатику та характеристики переходу, забезпечуючи прогностичну основу для проєктування високовольтних, кріогенних та надширокозонних напівпровідникових пристроїв.

Ключові слова: *n-тип β-Ga_2O_3; p-Si гетероперехід; неповна іонізація домішок; електростатика переходу; профілювання ємність–напруга; заморожування носіїв; температурно-залежний транспорт; кріогенна електроніка*